Optical Engineering

OpticalEngineering.SPIEDigitalLibrary.org

Long-range wind monitoring in real time with optimized coherent lidar

Agnes Dolfi-Bouteyre
Guillaume Canat
Laurent Lombard
Matthieu Valla
Anne Durécu
Claudine Besson

SPIE.

Agnes Dolfi-Bouteyre, Guillaume Canat, Laurent Lombard, Matthieu Valla, Anne Durécu, Claudine Besson, "Long-range wind monitoring in real time with optimized coherent lidar," *Opt. Eng.* **56**(3), 031217 (2016), doi: 10.1117/1.OE.56.3.031217.

Long-range wind monitoring in real time with optimized coherent lidar

Agnes Dolfi-Bouteyre, Guillaume Canat, Laurent Lombard, Matthieu Valla, Anne Durécu, and Claudine Besson*
Onera the French Aerospace Lab, Optics Department, 2 Chemin de la Hunière, 91123 Palaiseau, France

Abstract. Two important enabling technologies for pulsed coherent detection wind lidar are the laser and real-time signal processing. In particular, fiber laser is limited in peak power by nonlinear effects, such as stimulated Brillouin scattering (SBS). We report on various technologies that have been developed to mitigate SBS and increase peak power in 1.5-μm fiber lasers, such as special large mode area fiber designs or strain management. Range-resolved wind profiles up to a record range of 16 km within 0.1-s averaging time have been obtained thanks to those high-peak power fiber lasers. At long range, the lidar signal gets much weaker than the noise and special care is required to extract the Doppler peak from the spectral noise. To optimize real-time processing for weak carrier-to-noise ratio signal, we have studied various Doppler mean frequency estimators (MFE) and the influence of data accumulation on outliers occurrence. Five real-time MFEs (maximum, centroid, matched filter, maximum likelihood, and polynomial fit) have been compared in terms of error and processing time using lidar experimental data. MFE errors and data accumulation limits are established using a spectral method. [DOI: 10.1117/1.OE.56.3.031217]

Keywords: coherent lidar; Doppler lidar; laser; pulsed fiber amplifier; master oscillator, power fiber amplifier; frequency estimator.

Paper 161200SS received Jul. 28, 2016; accepted for publication Nov. 4, 2016; published online Dec. 6, 2016.

1 Introduction

New applications of Doppler lidars call for long range and short measurement time of range-resolved wind profiles. For example, in aeronautics, for safety concerns linked to the increase in air traffic flow, it is desired to monitor the air dynamics in the surrounding of airports. In these cases, the needed lidar products are wind velocity maps and the monitoring of turbulences. The requirement is to cover ranges longer than 8 km in a short acquisition time (360 deg map in 1 min). We have demonstrated that such data can be obtained thanks to fiber lidar technology.[1]

The performance of pulsed coherent Doppler wind lidars can be quantified, for a given measurement time (or averaging time), by its range limit (the farthest distance where we can extract reliable wind data) and its wind measurement accuracy for each range gate. Those quantities mostly depend on the lidar carrier-to-noise ratio (CNR) and signal processing. CNR depends on the laser power, the lidar optical architecture, the backscattering of the atmosphere at the time of measure, electronics, and acquisition/digitalization set up. We can define a quality factor K given as

$$K = \frac{E.\sqrt{\mathrm{PRF}}}{1 + (M^2)^2}, \tag{1}$$

where E is the pulse energy, PRF is the pulse repetition rate, and M^2 is the spatial quality factor of the Gaussian beam.[2] This factor K is proportional to the CNR of lidar data averaged over a given time.

From Eq. (1), several design rules can be inferred. First, the laser beam quality factor M^2 must be as close from 1 as possible ($M^2 = 1$ being the diffraction limit). Second, for a given laser average power, the CNR is optimized by increasing the energy per pulse rather than the pulse repetition frequency. On the other hand, the wind speed accuracy sets the minimum value of the pulse duration. Indeed, the wind speed measurement accuracy is related to the spectral width of the pulse. This calls for developing high-energy and high-peak power narrow linewidth laser sources, a technology enabler for the Doppler lidar. Wind lidars based on fiber laser technologies operate, however, in a regime with low-energy per pulse (typically, 10 μJ to 1 mJ) and high pulse repetition rate (PRF) (typically, 5 to 50 kHz). In this regime, the main peak power limitation is the stimulated Brillouin scattering (SBS) and special design strategies are necessary to increase the peak power. Onera has developed a specific know-how on high-peak power, narrow linewidth pulsed fiber lasers, and amplifiers thanks to various studies on SBS mitigation. They are described along with the obtained results in part 2 of this paper.

Although the most recent progress has been obtained by increasing the laser peak power, lidar performance improvements are also obtained by adapting the signal processing to the high PRF laser source. In this paper, "limit range" refers to the farthest distance where we can extract wind data. This limit range depends on the capability to extract the Doppler frequency at very low-signal level in order to push farther the last usable range gate. The purpose of the study exposed in part 3 is to select the best Doppler mean frequency estimator (MFE), i.e., an estimator reliable in very low CNR and fast enough for real-time display of long-range wind maps.

This paper is mostly a compilation based on results previously obtained by Onera and partners[3,4] on two objectives: the increase of the laser peak power and the

*Address all correspondence to: Claudine Besson, E-mail: claudine.besson@onera.fr

0091-3286/2016/$25.00 © 2016 SPIE

improvement of the lidar signal processing performance. Ways to achieve those objectives are:

- SBS mitigation techniques to increase the limit of the power in high-power fiber amplifiers;
- the introduction of a Doppler MFE and a comparison with commonly used estimators; and
- the introduction of a methodology to optimize the lidar limit range.

2 High Spectral Brilliance All Fibered Sources and Stimulated Brillouin Scattering Mitigation

2.1 *Lidar Requirements*

A typical coherent fiber lidar setup is depicted in Fig. 1. The master oscillator is a continuous laser diode that goes through an acousto-optic modulator (AOM), which shapes the pulse. It is then amplified through a fiber preamplification stage and a filter [bandpass filter (BPF)] and a booster stage. At the output of the booster stage, the beam is polarized; quasisingle mode and its temporal shape are optimized for efficient coherent detection. Most systems emit around 1545 nm, which corresponds to high gain in erbium-doped fibers, and a good atmospheric transmission. The assets of fiber lasers are their high efficiency enabling wall plug efficiencies of 10% to 15%, their size—the volume of a coherent 2-W fiber laser is the size of a thick book—and their reliability due to spliced connectors.

To reach long range within a short acquisition time, coherent wind lidars require high-peak power (500 W to 1 kW), narrow linewidth (few MHz) pulsed laser sources with nearly Fourier transform limited pulse duration (100 ns to 1 μs). Eyesafe, all-fiber laser sources based on master oscillator, power fiber amplifier (MOPFA) architecture offer many advantages over bulk sources, such as low sensitivity to vibrations, efficiency, and versatility. In the MOPFA coherent lidar setup shown in Fig. 1, the pulses are amplified in a sequence of fiber amplifier stages with increasing pump power and core size, which are separated by isolators and BPFs. MOPFA designers seek for fibers with low numerical aperture (NA), which is favorable to single-mode guiding and low amplified spontaneous emission (ASE) in order to get high system efficiency.

Narrow linewidth pulsed MOPFA is usually limited in peak power by nonlinear effects arising in the fiber, such as SBS to a few 10 to 100 s Watts in standard fibers.[5] In single-mode fibers, the SBS threshold is reached when the peak power time length product reaches $\sim$80 W $\cdot$ m. The high-power density generates acoustic waves into the fiber core, which acts as a grating. The light transmitted by the fiber saturates and part of this light is backscattered by the grating. In fiber amplifiers, the backscattered light may be amplified into the active fiber generating high-peak power backscattered pulses potentially harmful for beforehand components.[6]

The strength of the Brillouin nonlinearities in a fiber can be quantified by the intensity length product B:[7]

$$B = g_B \frac{\int_0^L P(z)\mathrm{d}z}{A_{\mathrm{eff}}} = \frac{g_B P(L) L_{\mathrm{eff}}}{A_{\mathrm{eff}}}, \tag{2}$$

where g_B is the Brillouin gain, L is the fiber length, A_{eff} is the effective area of the fundamental mode, $P(z)$ is the signal power distribution along the fiber, and L_{eff} is the effective length. For passive fiber, the effective length is equal to the physical fiber length, and for active fiber, the effective length depends on the fiber gain along the fiber. To increase the achievable peak power at amplifier output, B must be increased. From Eq. (2), it appears that there are three ways to act on the nonlinearities.

2.2 *Increase of Mode Area*

The first way is to increase the fundamental mode effective area. Large mode area (LMA) fibers, with large core diameter and low NA, may be used to increase the mode area. However, LMA fibers tend to guide higher-order transverse modes and degrade the beam quality, which is crucial for many applications. For instance, in a coherent detection lidar, Eq. (1) shows that when the beam quality factor M^2 is increased from 1 to 1.7, the CNR is expected to decrease by 3 dB. Thus, a compromise has to be found between nonlinear effects and beam quality.

The most efficient doped fibers today are based on the erbium–ytterbium codoping of phosphosilicate glasses. This composition has two important limitations. First, the core refractive index is quite large and special pedestal structures are needed to reduce the NA down to 0.09 and limit the proportion of higher-order transverse modes. A second limitation is that the core itself is usually inhomogeneous with a central dip in the refractive index profile resulting in a poor beam spatial quality.

To go beyond this core diameter limit, Leibniz-Institut für Photonische Technologien Jena, Germany, and Onera have built a 40-μm core diameter multifilament-core fiber (MFC) to amplify high-peak power pulses.[8] In this technology, the fiber core is replaced by a microstructured core composed of 37 erbium–ytterbium-doped filaments surrounded by fluorine doped silica. It was shown that this structure behaves as an effectively single-mode fiber as the light sees only

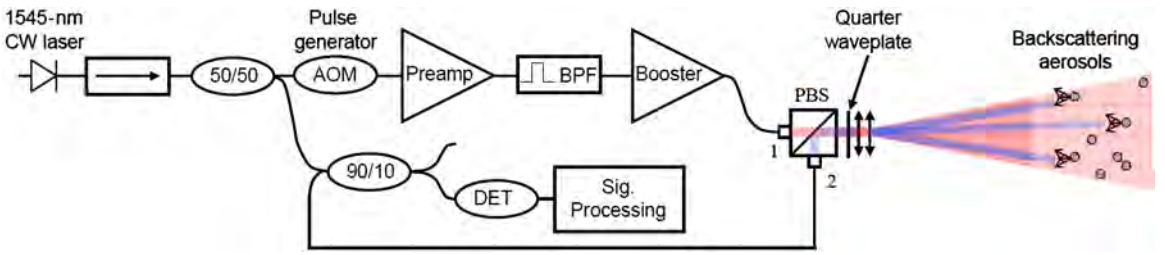

Fig. 1 MOPFA coherent fiber LIDAR setup. AOM, acousto-optics modulator; BPF, bandpass filter; PBS, polarization beam splitter; and DET, detector.

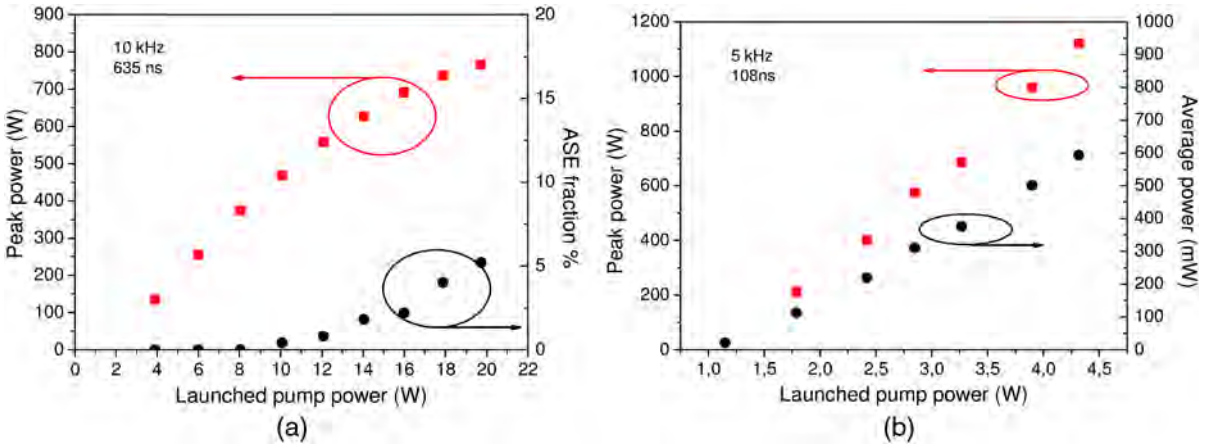

Fig. 2 Pulse peak power with respect to launched pump power in the pulsed setup. (a) Pulse duration = 635 ns and PRF = 10 kHz. The ASE fraction in total power is shown on the right axis. (b) Pulse duration = 108 ns and PRF = 5 kHz. The average power is shown on the right axis.

an average index value for the structured core. Pulses with 940-W peak power, 1-μs duration, and 1-MHz laser linewidth were achieved. The beam quality was good with $M^2 \sim 1.3$. However, this laser setup was not all-fiber. Indeed MFC fiber manufacture and integration in all-fiber lasers systems are challenging.

Another method to increase the core size while preserving a good beam quality is to change the core composition. We have tested phosphoaluminosilicate glass fibers (PAS). It has been previously demonstrated that the simultaneous codoping by alumina and phosphorous results in the reduction of the refractive index leading to lower NA cores.[9,10] We have tested a double-cladding PAS erbium–ytterbium-doped fiber with a 30-μm diameter core with a pedestal and 300-μm inner cladding. The core NA is 0.09 with respect to the pedestal. This fiber can be highly doped and we managed to make an efficient power amplifier with a short piece of fiber only 2-m long. When the pump power is increased, the pulse peak power is increasing steadily up to 770-W peak power corresponding to a 650-ns pulse energy of 450 μJ [Fig. 2(a)]. The ASE fraction in the total output power is 6% at that point and the slope efficiency is 23%. For 108-ns pulses, the peak power is increased up to the SBS threshold at 1120 W [Fig. 2(b)]. The ASE fraction is then below 1%.

2.3 *Strain Distribution*

A second way to decrease the Brillouin effect is to minimize the integral of the power over the fiber length. By definition, this term is also equal to the product of fiber output power times effective length L_{eff}. In a standard fiber, all the fiber length contributes to Brillouin reflectivity at the same characteristic frequency. A strain gradient applied along the fiber can be used to make each fiber segment contribute to different frequencies and spread the reflected light spectrum[11] thus allowing higher optical peak power in the fiber before reaching the Brillouin threshold.

We have recently developed a high-power single-frequency all-fiber MOPFA using high reliability passive components and this strain technique. This MOPFA was used in the first experimental demonstration of a fiber laser-based wind lidar with more than 10-km range.[12] We have been able to spread the light reflected by a 25-μm core fiber resulting in an increase of more than 3 dB on the SBS threshold. Without the strain gradient, SBS limits the pulse peak power to 300 W (200 μJ per 600-ns pulses). The M^2 is measured to be less than 1.3 in both axes. With the strain gradient applied

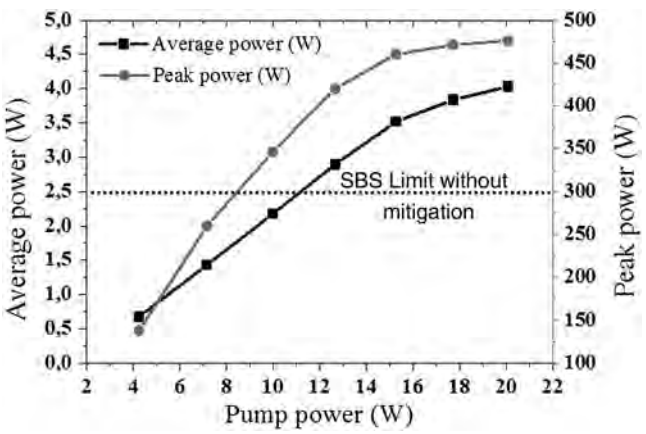

Fig. 3 Evolution of the average power and peak power out of the high-power amplifier with fiber straining. Dotted line: amplifier maximum peak power without strain implementation.

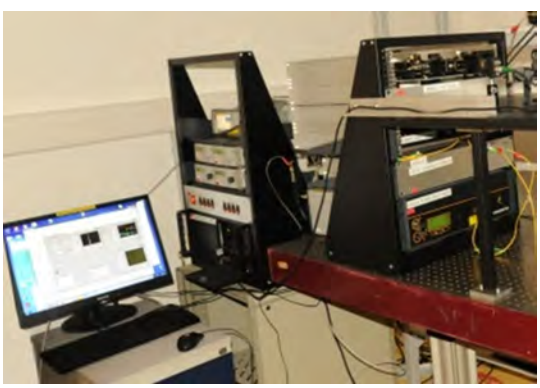

Fig. 4 The integrated engineering model of fiber laser HEPILAS for CO_2 monitoring from space.

to the doped fiber, peak power up to 630 W was achieved (350 μJ per 550-ns pulses) (see Fig. 3).

Since then, this technique has been applied to design high energy pulsed fiber lasers (HEPILAS) a high-power laser emitting at 1579 nm for space application (see Fig. 4). The aim of the European Space Agency project was to study a proof of concept for monitoring CO_2 from space with a differential absorption lidar based on an all-fiber laser. The 1.7-kW peak power was obtained for 150-ns pulses with excellent beam pointing stability. A factor of 3 gain was obtained with a modest value of strain so as to ensure that the fiber lifetime was compatible with a 5-year duration space mission. The laser was also designed so as to withstand 10-kRad radiations thanks to iXfiber radhard active fiber.[13]

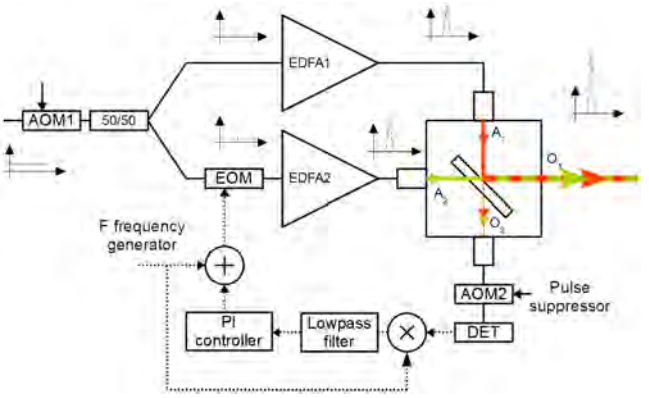

Fig. 5 Coherently combined pulsed amplifier setup. Output O1 carries the total power of outputs A1 and A2. AOM1 and AOM2, acousto-optic modulators; EDFA1 and EDFA2, fiber amplifiers; EOM, electro-optic modulator; PD, photodiode; and PI, proportional-integral control loop.

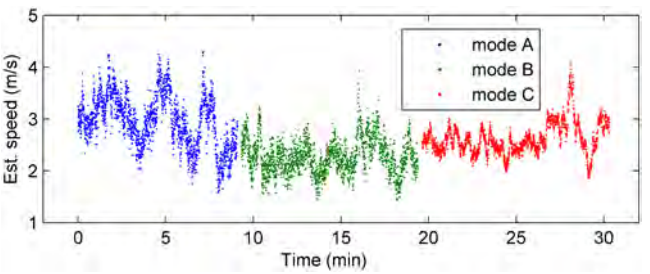

Fig. 6 Estimated wind speed (m/s) time series as recorded by the wind lidar in configurations A, B, and C.

2.4 *Coherent Combining*

The third strategy to tune Eq. (2) is to coherently add up the energy emitted by several fibers limited by SBS while preserving the good beam quality. Coherent beam combination (CBC) allows improving the output power of MOPFA sources by adding the outputs of single amplifiers. To achieve this, two or more amplifiers seeded by the same pulsed oscillator are coherently combined into a single-mode beam. To achieve high CBC efficiency, the phase differences are compensated using a controller. We have demonstrated CBC of two amplifiers in a 100-ns pulse regime limited to 95 and 123 W, respectively, resulting in peak power of 208 W.[14] Beam quality and spectral linewidth were maintained. This source has been successfully tested in a lidar configuration.[15] The setup of the CBC of two pulse amplifiers is shown in Fig. 5.

In particular, we demonstrated that the pulse operation CBC phase controller does not impair the lidar performances. Indeed, the source of Fig. 5 has been used as a booster in a lidar setup with 240-ns pulse duration. We have compared the lidar performances when running (A) one amplifier at full power, (B) two amplifiers at half power, and (C) two amplifiers at full power. The estimated wind speed time series are shown in Fig. 6. Modes A and B show similar estimated speed variance while mode C shows a reduced estimated speed variance.

The power spectral densities (PSDs) of each recorded time evolutions are reported in Fig. 7. The extracted noise floors (0.21 m/s for mode A, 0.19 m/s for mode B, and 0.08 m/s for mode C) show that no performance degradation has been measured when using CBC. When both amplifiers are run at full power, the expected lidar performance improvement is reached. In all cases, the lidar performance is close to its optimum given by the Cramer–Rao bound.[16]

Those results show the compatibility of coherent beam combining with coherent wind lidar. Theoretically, up to hundreds of those amplifiers can be combined by this technique.

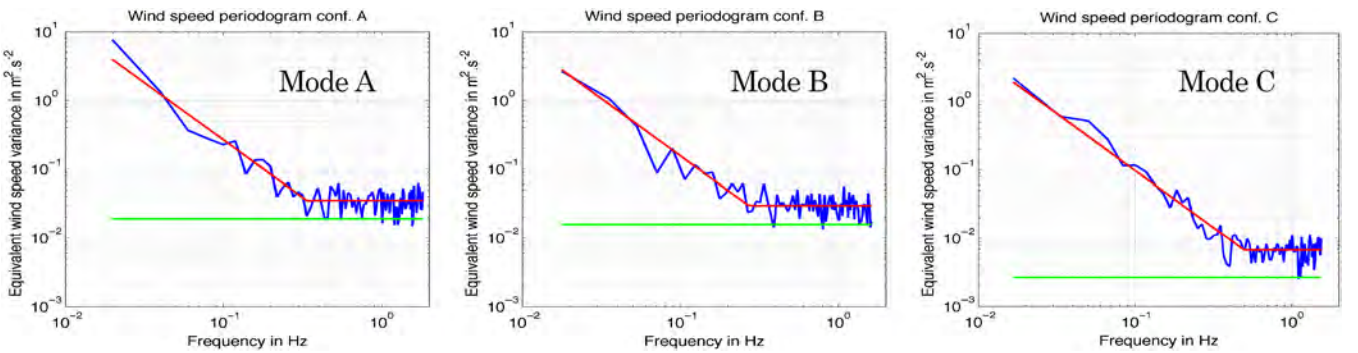

Fig. 7 Lidar performance comparison at 150 m—instrument noise floor comparison; blue: PSD of estimated wind speed from Fig. 6; red (low frequency): $\alpha f - 5/3$ Kolmogorov law (α fitted to data); red (high frequency): lidar noise floor fitted to data; and green: lidar theoretical noise floor from estimated CNR (Cramer–Rao bound).

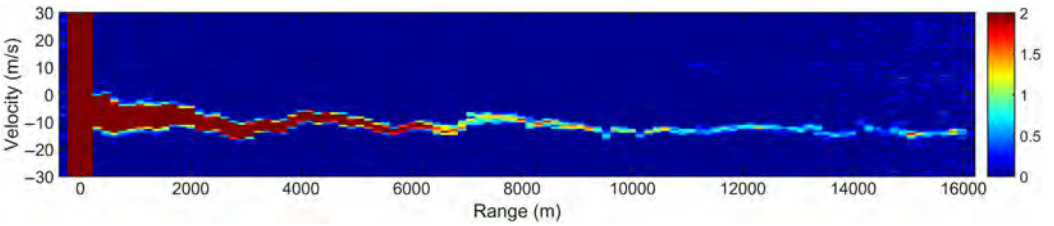

Fig. 8 Wind speed (wind speed in m/s) spectrograms versus range (m). Color scale is the PSD in 0.1-s average time.

2.5 *Long-Range Lidar Measurements*

Building wind lidars based on these high-power sources enabled achieving 16-km-record range[17] in 2015. Onera wind lidar system LICORNE is based on the architecture shown in Fig. 1 and can integrate various high-power sources or components for tests. A sample wind speed spectrogram is shown in Fig. 8 in a fixed line of sight configuration. The range gates are reported on x-axis and for a given range gate, columns show lidar data PSD averaged over 1024 spectra, corresponding to 0.1-s acquisition time (see Sec. 3.1). The color scale is chosen to reveal Doppler peak at longer distance and saturates at shorter distance. CNR at a given distance is the ratio of the power contained in this Doppler peak to the power contained in the background noise. At longer distance, the background noise increases due to ASE originating from the laser. Both the decrease of the Doppler peak intensity with distance and the increase of this additional noise with distance limit the CNR and thus the lidar range. The spectrogram shows that ranges beyond 15 km are achieved with 0.1-s averaging time.

The MFE estimates the Doppler peak location for each distance, yielding to range-resolved estimated velocity.

3 Signal Processing Optimization

The high gain achieved by high-power fiber amplifiers generates levels of spectrally broad ASE, which are not negligible in the power budget of the lidar, overcoming other noise contributors (essentially the limiting local oscillator shot noise) and thus limiting the CNR. Indeed, because of continuous pumping, the gain in the amplifiers increases between the pulses to reach a maximum before a pulse. Similarly, after the pulse emission, the ASE builds up and reaches its highest level just before the next pulse emission, simultaneously with the farthest range gates signal detection. The spurious ASE signal emission between pulses is all the more critical as the Doppler signal is weakest at long-range gates. Thus, for long-range wind lidar design, ASE emission is a critical parameter of the MOPFA chain to be taken care of. However, the Doppler peak extraction from the background noise remains a tricky part of the long-range lidar optimization. Note that the lag angle limitation for long-range fast scanning lidar[18] is not considered in this work.

Several types of algorithms can be used to process coherent lidar wind experimental data with low CNR. We have conducted a systematic study on the signal processing in order to choose the optimal processing algorithm and its parametrization. Because real-time display of wind maps is mandatory for most applications, we considered only simple and/or quick MFE. Five different algorithms have been implemented and compared on the same set of lidar data: maximum, centroid, parabolic fitting, maximum likelihood, and adapted filtering. The Cramer–Rao bound (theoretical best performance) has also been computed. Data have been acquired with a fixed beam (no scanning) middle range lidar (1.5 to 2 km).

Table 1 Lidar characteristics necessary to the data set analysis.

Pulse duration	400 ns	Sampling rate Fs	500 MHz
PRF	14 kHz	Total number of acquired points per pulse	12 288
Intermediate frequency fit	120 MHz	FFT length N	512
Maximum range	3500 m	Zero-padding factor	1 or 4
		Reduced bandwidth for numerical frequency analysis[a]	[90 150] MHz

[a]PSD bins outside this bandwidth are discarded; the accessible wind range is ±23 m/s.

Table 1 gives the main useful lidar characteristics for the data set analysis.

3.1 *Algorithms Description*

The backscattered signal is acquired for each pulse. A PSD is computed for each distance and laser shot using a discrete Fourier transform (DFT) with zero padding. The PSD is the squared modulus of the DFT. Before any operation, a noise floor measured from data recorded before laser emission is removed. PSD analysis includes an estimation of the CNR, defined as the ratio of the power contained in the signal to the power contained in the noise over the full detector bandwidth, and an estimation of the wind speed through one of the five estimators.

3.1.1 *Zero padding*

Frequencies in the DFT are spaced at intervals of F_s/N, where Fs is the sample rate and N is the number of samples in each input time series. Frequency estimation by peak search results in a speed accuracy limited by the frequency resolution. Zero-padding data before performing DFT artificially increase the frequency resolution by adding zeros to the time series so as to obtain NFFT samples. The resulting interpolation is smoother and the peak search more precise. Zero padding of 1 performs the FFT over the next power of

two from N ($N1$); zero padding of 4 performs the FFT over $4 \times N1$ samples.

3.1.2 *Power spectral density accumulation*

Fiber laser operates at high PRF, allowing an averaging over a large number of spectra in order to reduce speckle noise. For the analyzed lidar data, PRF is equal to 14 kHz and 1024 spectra are averaged on a current base corresponding to a measurement time of 70 ms. This enables very efficient noise reduction. Figure 9 shows an example of averaged PSD at very low CNR (−23 dB) for an averaging over 32 and for an averaging over 1024. The average noise level is also displayed (yellow). Zero padding is equal to 4.

3.1.3 *Maximum estimator*

Maximum estimator or peak search is the simplest estimator and consists of selecting the point in the average PSD with the highest power density. The accuracy of the algorithm directly depends on the zero padding level. All the following algorithms except for the adapted filter take the result of the maximum estimator as a starting point.

3.1.4 *Centroid or barycenter estimator*

Computing the moments of the average PSD gives access to the CNR (zero-order moment), Doppler frequency (first-order moment), and wind dispersion (second-order moment after rectification from the frequency broadening due to the pulse length and DFT window size).

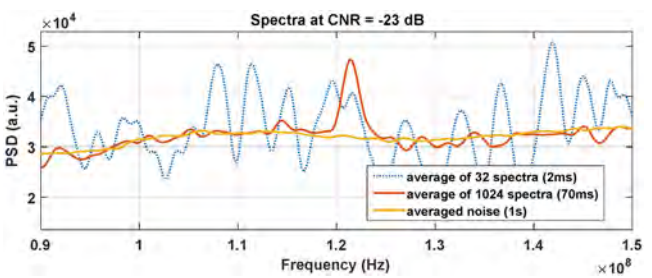

Fig. 9 Example of PSD accumulation.

3.1.5 *Parabolic fitting estimator*

For Doppler lidar with short pulse (<500 ns) in laminar wind conditions (wind shear and wake-vortex conditions are excluded), and assuming a Gaussian pulse shape and a Gaussian DFT window, the spectral shape of the theoretical PSD is close to Gaussian. The logarithm of the average PSD is a parabola that can be adjusted to the measured PSD. The fitted parabola center, integral, and FWHM give the Doppler frequency, the CNR, and the wind dispersion, respectively.

3.1.6 *Maximum-likelihood estimator*

The maximum-likelihood estimator (MLE) has been adapted to pulsed Lidar.[18,19] A model of the lidar signal is necessary for MLE. We have chosen a signal model based on the "feuilleté" model[20] for laminar wind conditions, taking into account the shape of the lidar pulse. The signal model has three free parameters: the CNR, the Doppler shift, and the spectral width. The MLE consists of finding the value of these free parameters (CNR, Doppler shift, and spectral width), which maximizes the joint probability of the signal. The implemented MLE assumes that spectral bins are not correlated. More details are available in Refs. 18 and 16. Due to the lidar model complexity, processing time of MLE is the most demanding.

3.1.7 *Adapted filter estimator*

An adaptive filter for frequency estimate of heterodyne Doppler lidar returns has been proposed by Zarader et al.[21] Further implementation was proposed by Dabas et al.[22] This adaptive filter removes the atmospheric contribution from noise. For fiber laser with a high PRF, spectral averaging has already removed a large quantity of noise, and the algorithm is less efficient than for low PRF lidar.

3.2 *Outliers Filtering*

In this work, outliers (or bad estimates) are defined by wind speed values that are distant from surrounding measurements. Generally, the range of wind lidars is limited by outliers that appear when the signal peak in the spectrum becomes close to the noise level, thus impairing peak search. All but adapted filter MFEs are initiated by a peak search and

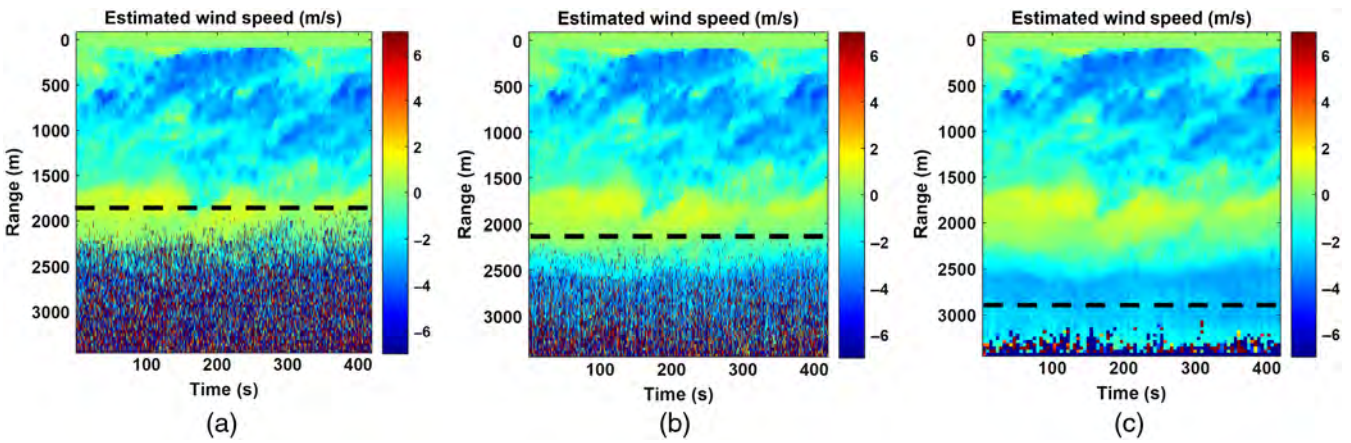

Fig. 10 Color velocity map evaluated with centroid estimator, for (a) 1024, (b) 4096, and (c) 65536 accumulated PSD. X-axis is time (s) and Y-axis is range (m). Horizontal dashed line shows the limit range defined by the zero-outlier criterion.

thus suffer from the same limitation. A usual method to reduce outlier occurrence is to search for the peak frequency within a limited bandwidth around the heterodyne frequency (± 30 MHz $\Leftrightarrow 48 \pm 23$ m/s in our case). To further reduce outlier occurrence, one can increase the PSD accumulation as seen in Fig 9. Figure 10 shows the evolution in limit range (defined as first appearance of outliers) in a data set when averaging 1024 (70 ms), 4096 (0.28 s), and 65536 spectra (4.6 s), respectively. As expected, the limit range increases with the number of accumulated PSD M (Fig. 10).

3.2.1 *Outlier ratio*

We define an outlier ratio b as the probability to obtain an outlier per peak search. $b \to 0$ at high CNR (short distance) $b \to 1$ at low CNR (long distance). The following relation is derived from the empirical equation established by Frehlich[23] (Eq. 23) for a given noise bandwidth

$$\mathrm{CNR} = \frac{f(b)}{\sqrt{M}}, \tag{3}$$

where M is the number of accumulated PSD and f is an increasing function of b. This relation gives the required CNR to achieve an outlier ratio b. In other words, for a given outlier ratio b, the product $\mathrm{CNR} \cdot \sqrt{M}$ is constant. f can be experimentally evaluated and depends only on lidar configuration. To experimentally verify the relation between limit range, CNR and M, we identified the distance (and the corresponding measured CNR) of the appearance of the first outlier ($b \to 0$) on the dataset of Fig. 10 for various values of M. The results are reported in Fig. 11(a) (red crosses). As expected from Eq. (3), for a fixed b, the product $(\mathrm{CNR} \cdot \sqrt{M})$ is constant. In Fig. 11(b), we report measured outliers ratio b as a function of range for various values of M. It highlights the limit range increase with accumulation.

The increase in limit range with M is, however, limited by the coherence time of wind speed, which is related to atmospheric stability. Indeed, wind velocity variation within the averaging time can degrade PSD contrast. The optimal accumulation time, for a given range and a given atmosphere, can be obtained by drawing the PSD of wind data (Fig. 12). Wind data fluctuation is the consequence of wind turbulence and follows a Kolmogorov law and its PSD is proportional to $f^{-5/3}$.[24] Figure 12 shows the PSD of the wind data set computed at 1300-m range for averaging times corresponding to Fig. 10. On the PSD log–log graph, we can visualize the $-5/3$ slope of the wind turbulence, and the flat level of the estimator noise.[25] To obtain the estimated wind speed error, the noise floor level is integrated over the full bandwidth of the measurement. The position of the PSD elbow gives the optimal accumulation time (i.e., the frequency cutoff)

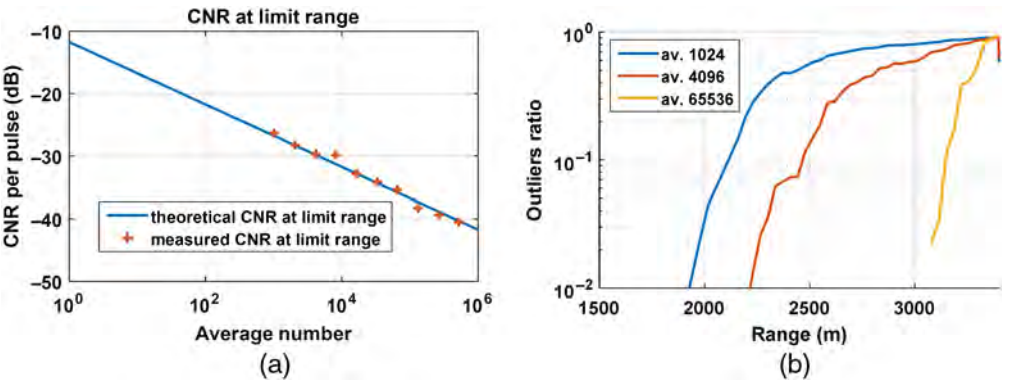

Fig. 11 (a) Theoretical number of accumulated PSD (M) required for zero outlier for a given CNR (blue curve). Experimental CNR at limit range (red crosses). (b) Outliers ratio A versus range for different M. Velocities were estimated using centroid algorithm. Note that CNR and range are experimentally related through the unknown backscattering coefficient beta.

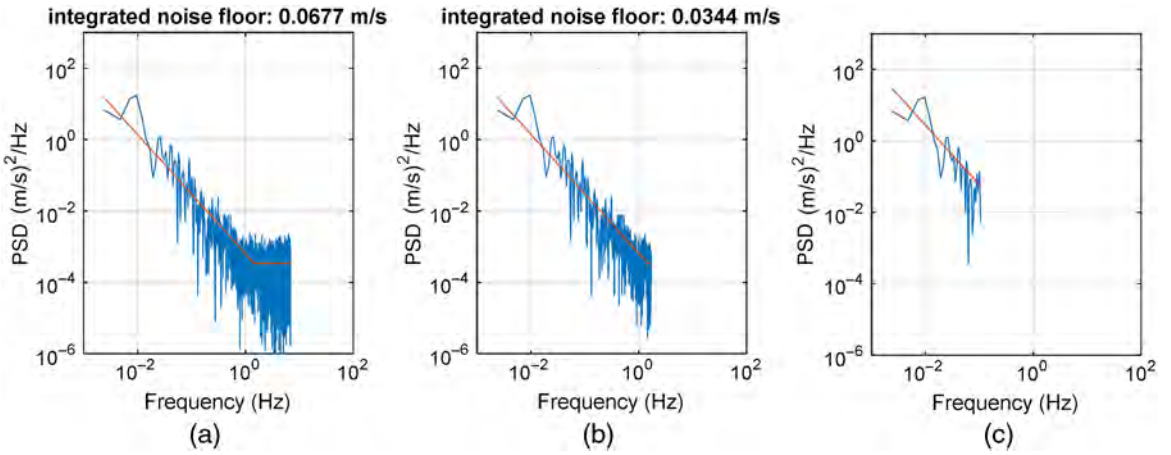

Fig. 12 Wind PSD for various accumulation time: (a) 70 ms, (b) 0.28 s, and (c) 4.6 s.

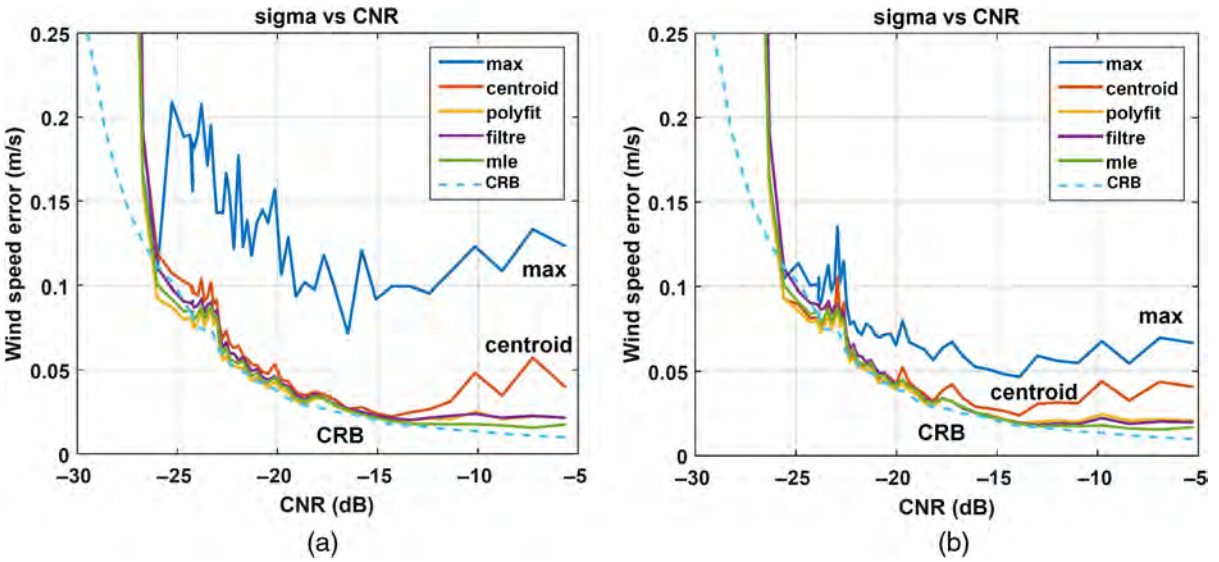

Fig. 13 Estimators accuracy as a function of CNR (a) without and (b) with zero padding for 70-ms accumulation time.

beyond which accuracy is not improved any more. It is dependent on the range and on the atmosphere state. Information on wind is lost when averaging above this limit as exemplified in Fig. 12(c). To sum up, in the case of Fig. 12, data can be accumulated up to 0.28 s with no information loss. For a longer accumulation time, part of the information is lost.

3.3 *Algorithm comparison*

The estimated wind speed error is computed with the above procedure for each range gate and for the five estimators using the PSD of the velocity data (see Fig. 12) in order to compare the estimator accuracy. The results are shown in Fig. 13 without (a) and with (b) zero padding as a function of CNR. A turbulent event appears for the range gate corresponding to CNR $= -23$ dB and degrades all estimators variance. The theoretical performance of the wind speed estimator, given by Cramer–Rao bound,[18,16] has been computed from CNR estimated values and is illustrated by the dash blue line in Fig. 13.

The parametric estimators (polynomial fit and MLE) do not require zero padding to reach a good accuracy (within Cramer–Rao bound accuracy). On the contrary, nonparametric (maximum and centroid) estimators are improved with zeros-padding; centroid estimator can even reach the same level of accuracy as the parametric estimators. Filter estimator performances are comparable with MLE and polynomial fit performances.

Regarding computing time, maximum, centroid, and polynomial fit estimators are much less computing intensive than the MLE estimator. However, most of the processing time is dedicated to spectra computing and accumulation. The spectrum computing time even increases with zero padding and with laser PRF (high in our case). Table 2 summarizes the results of the compared estimators in terms of performances and overall computing time (including spectra computing and wind estimation).

To conclude, in our study case, a high PRF lidar and laminar wind field analysis, the best candidate is the polynomial fit estimator on spectra computed without zero padding.

Table 2 Estimators performances summary.

	Estimation computing time	Accuracy with zero padding	Accuracy without zero padding	Overall computing time for good accuracy
Maximum	Short	Medium	Bad	N/A
Centroid	Short	Good	Medium	Long
Polynomial fit	Short	Good	Good	Shortest
MLE	Long	Good	Good	Longest
Adapted filter	Medium	Good	Good	Medium

4 Conclusion

Two of the most important enabling technologies for pulsed coherent detection wind lidar are the laser and the real-time signal processing. Regarding the laser, we have investigated various SBS mitigation techniques to overcome nonlinear optics limitations and improve the peak power of coherent lidar sources. They have been integrated in MOPFA architectures yielding record peak power for narrow linewidth pulses with low fraction of ASE and excellent beam quality. The 1120-W peak power and 108-ns pulses were achieved using PAS erbium–ytterbium-doped fiber with 30-μm diameter. The 630-W peak power and 550-ns pulses were achieved using Onera strain gradient technique. Peak power can be further increased thanks to coherent beam combining of several fiber lasers and the principle of a wind lidar based on this technology has been proven.

Onera wind lidar based on these high-power, high spectral brightness, all-fiber sources have achieved a horizontal air speed profiling up to 16 km in 0.1 s. The additional laser power provides increased lidar capability in range and

scanning of large areas but also better system resistance to adverse weather conditions by maintaining a high level of good velocity estimates.

Regarding the signal processing, we propose a methodology to optimize the lidar data accumulation time, which may be applied among others to long-range lidar based on high PRF MOPFA. A relation between the accumulation time and the CNR value to ensure a given acceptable outlier ratio has been presented and this relation has been verified experimentally with a middle range lidar.

The performances of five Doppler frequency estimators have been evaluated and their total processing time compared. For our study case (high PRF lidar and laminar wind field analysis), the best candidate is the polynomial fit estimator without zero padding. In the case of more complex wind field analysis (e.g., wake vortex), zero padding or more complex parametric estimators are required.[26]

Next lidar developments should benefit from these results. Indeed, with increased limit range and higher data refresh rate, lidar can offer improved capability for air speed and gas fluxes monitoring for application in the field of airport safety, aircraft navigation, or green gas surveillance.

Acknowledgments

The authors would like to acknowledge the Conseil Général de l'Essonne for funding the ASTRE MUSEON, the campus Paris-Saclay for funding LICOFIM, DGCIS for funding FEYMOUS and the European Commission for funding FP7/UFO. The authors would like to thank Yves Jaouen, iXfiber, Keopsys, Leosphere, and Thales for fruitful collaboration.

References

1. F. Barbaresco et al., "Monitoring wind, turbulence and aircraft wake vortices by high resolution RADAR and LIDAR remote sensors in all weather conditions," in *Proc. of URSI-France*, wakenet.eu (2015).
2. J.-P. Cariou, B. Augere, and M. Valla, "Laser source requirements for coherent lidars based on fiber technology," *C. R. Phys.* **7**(2), 213–223 (2006).
3. N. Cezard et al., *1579 nm Fiber Laser Source*, ILRC, New York (2015).
4. L. Lombard et al., "Performance of frequency estimators," in *CLRC 18th Coherent Laser Radar Conf.*, CLRC, Boulder (2016).
5. G. Canat, Y. Jaouën, and J.-C. Mollier, "Performance and limitations of high brightness $Er^{+}3 - Yb^{3+}$ fiber sources," *C. R. Phys.* **7**(2), 177–186 (2006).
6. G. Kulcsar et al., "Multiple-Stokes stimulated Brillouin scattering generation in pulsed high-power double-cladding Er/sup 3+/-Yb/sup 3+/-codoped fiber amplifier," *IEEE Photonics Technol. Lett.* **15**(6), 801–803 (2003).
7. Y. Jaouën et al., "Power limitation induced by nonlinear effects in pulsed high-power fiber amplifiers," *C. R. Phys.* **7**(2), 163–169 (2006).
8. G. Canat et al., "Multifilament-core fibers for high energy pulse amplification at 1.5 μm with excellent beam quality," *Opt. Lett.* **33**(22), 2701–2703 (2008).
9. G. G. Vienne et al., "Role of aluminum in ytterbium–erbium codoped phosphoaluminosilicate optical fibers," *Opt. Fiber Technol.* **2**(4), 387–393 (1996).
10. A. N. Abramov et al., "Fabrication of heavily Er_2O_3 doped aluminophosphosilicate glass fibers," *Inorg. Mater.* **46**(4), 439–444 (2010).
11. J. M. C. Boggio, J. D. Marconi, and H. L. Fragnito, "Experimental and numerical investigation of the SBS-threshold increase in an optical fiber by applying strain distributions," *J. Lightwave Technol.* **23**(11), 3808–3814 (2005).
12. W. Renard et al., "Beyond 10 Km range wind-speed measurement with a 1.5 μm all-fiber laser source," in *Conf. on Lasers and Electro-Optics (CLEO 2014)*, San Jose, Paper No. AW1P.5 (2014).
13. G. Canat et al., "High peak power single frequency amplifiers based on efficient erbium–ytterbium doped LMA fibers," in *2015 European Conf. on Lasers and Electro-Optics—European Quantum Electronics Conf.*, Paper No. CJ_12_5 (2015).
14. L. Lombard et al., "Coherent beam combination of narrow-linewidth 1.5 μm fiber amplifiers in a long-pulse regime," *Opt. Lett.* **36**(4), 523–525 (2011).
15. L. Lombard et al., "Eyesafe coherent detection wind lidar based on a beam-combined pulsed laser source," *Opt. Lett.* **40**(6), 1030–1033 (2015).
16. B. J. Rye, "Estimate optimization parameters for incoherent backscatter heterodyne lidar including unknown return signal bandwidth," *Appl. Opt.* **39**, 6086–6096 (2000)
17. L. Lombard et al., "Long range wind lidars based on novel high spectral brilliance all-fibered sources," *Proc. SPIE* **9645**, 96450B (2015).
18. R. Frehlich, "Scanning doppler LIDAR for input into short-term wind power forecasts," *J. Atmos. Oceanic Technol.* **30**, 230–244 (2013).
19. M. Valla et al., "Fourier transform maximum likelihood estimator for distance resolved velocity measurement with a pulsed 1.55 μm erbium fiber laser based lidar," in *Proc.13th Coherent Laser Radar Conf. (CLRC 2005)*, Kamakura (2005).
20. P. Salamitou, A. Dabas, and P. Flamant, "Simulation in the time domain for heterodyne coherent laser radar," *Appl. Opt.* **34**(3), 499–506 (1995).
21. J. L. Zarader et al., "Velocity biases of adaptive filter estimates in heterodyne Doppler lidar measurements," *J. Atmos. Oceanic Technol.* **13**, 16–28 (1996).
22. A. M. Dabas, P. Drobinski, and P. Flamant, "Adaptive filters for frequency estimate of heterodyne Doppler lidar returns: recursive implementation and quality control," *J. Atmos. Oceanic Technol.* **16**(3), 361–372 (2000).
23. R. Frehlich, "Simulation of coherent Doppler lidar performance in the weak-signal regime," *J. Atmos. Oceanic Technol.* **13**(3), 646–658 (1996).
24. S. Monin and A. M. Yaglom, *Statistical Fluid Mechanics: Mechanics of Turbulence*, 1st ed., Vol. **2**, p. 874, Courier Corporation (1975).
25. R. Frehlich, S. M. Hannon, and S. W. Henderson, "Coherent Doppler lidar measurements of wind field statistics," *Boundary Layer Meteorol.* **86**, 233–256 (1998).
26. A. Hallermeyer et al., "Development and assessment of a wake vortex characterization algorithm based on a hybrid LIDAR signal processing," in *8th AIAA Atmospheric and Space Environments Conf.*, Washington (2016).

Agnes Dolfi-Bouteyre graduated from Ecole Superieure d'Optique, Orsay, in 1986 and received her PhD in physics from University Paris XI in 1990. She joined Onera in 1990, where she has been involved in laser and lidar system development for defense and aerospace. Her current areas of interest and specialization are lidar, coherent lidar, atmospheric turbulence measurement, aircraft wake-vortex detection, and lidar signal processing.

Guillaume Canat graduated from the Ecole Polytechnique, Palaiseau in 2000. He did his PhD thesis at the Ecole Nationale Supérieure de l'Aéronautique et de l'Espace in 2006. He has been a research scientist at Onera since 2002. His research interests include high-power fiber laser sources, nonlinear effects in fibers, and coherent combining.

Laurent Lombard received his engineering diploma from the Ecole Superieure d'Optique, Institut d'Optique, Orsay, France, in 2002 and his PhD from the University of Paris XI, France, in 2005. Since 2006, he has been a research scientist at Onera, Palaiseau, France. His current research deals with high-power fiber lasers, lidars, and optical beam processing.

Matthieu Valla received engineering and PhD degrees from Telecom Paristech, Paris, France, in 2001 and 2005, respectively. He has been working as a research engineer at Onera since 2002.

Anne Durécu graduated from the Institut National des Télécommunications in 2001 and received her PhD in optics from the Université de Limoges in 2005. She joined Onera in 2005 as a research scientist. She has been working on fiber laser development for lidar systems and on the potential of lasers for defense applications.

Claudine Besson obtained her PhD in physics from Optics Graduate School in 1989. She is a senior scientist and Sources Laser et Systèmes Lidar group leader at Onera. Her current fields of interest are fiber lasers and lidars.